

Edinburgh 2011/15  
 IFUM-981-FT  
 FR-PHENO-2011-013  
 RWTH TTK-11-32

## Reweighting and Unweighting of Parton Distributions and the LHC W lepton asymmetry data

### The NNPDF Collaboration:

Richard D. Ball<sup>1</sup>, Valerio Bertone<sup>2</sup>, Francesco Cerutti<sup>3</sup>, Luigi Del Debbio<sup>1</sup>,  
 Stefano Forte<sup>4</sup>, Alberto Guffanti<sup>2,5</sup>, Nathan P. Hartland<sup>1</sup>, José I. Latorre<sup>3</sup>, Juan Rojo<sup>4</sup>  
 and Maria Ubiali<sup>6</sup>.

<sup>1</sup> *Tait Institute, University of Edinburgh,*

*JCMB, KB, Mayfield Rd, Edinburgh EH9 3JZ, Scotland*

<sup>2</sup> *Physikalisches Institut, Albert-Ludwigs-Universität Freiburg,*

*Hermann-Herder-Straße 3, D-79104 Freiburg i.B., Germany*

<sup>3</sup> *Departament d'Estructura i Constituents de la Matèria, Universitat de Barcelona,*  
*Diagonal 647, E-08028 Barcelona, Spain*

<sup>4</sup> *Dipartimento di Fisica, Università di Milano and INFN, Sezione di Milano,*  
*Via Celoria 16, I-20133 Milano, Italy*

<sup>5</sup> *The Niels Bohr International Academy and Discovery Center,*

*The Niels Bohr Institute, Blegdamsvej 17, DK-2100 Copenhagen, Denmark*

<sup>6</sup> *Institut für Theoretische Teilchenphysik und Kosmologie, RWTH Aachen University,*  
*D-52056 Aachen, Germany*

### Abstract:

We develop in more detail our reweighting method for incorporating new datasets in parton fits based on a Monte Carlo representation of PDFs. After revisiting the derivation of the reweighting formula, we show how to construct an unweighted PDF replica set which is statistically equivalent to a given reweighted set. We then use reweighting followed by unweighting to test the consistency of the method, specifically by verifying that results do not depend on the order in which new data are included in the fit via reweighting. We apply the reweighting method to study the impact of LHC W lepton asymmetry data on the NNPDF2.1 set. We show how these data reduce the PDF uncertainties of light quarks in the medium and small  $x$  region, providing the first solid constraints on PDFs from LHC data.

# Contents

<b>1</b>	<b>Introduction</b>	<b>3</b>
<b>2</b>	<b>Reweighting</b>	<b>5</b>
2.1	Integration over the data space . . . . .	5
2.2	Weights for a given $\chi$ . . . . .	6
2.3	Multiple experiments . . . . .	7
<b>3</b>	<b>Unweighting</b>	<b>9</b>
3.1	The unweighting method . . . . .	10
3.2	Testing unweighting . . . . .	12
<b>4</b>	<b>Consistency</b>	<b>15</b>
4.1	Multiple Reweighting . . . . .	15
4.2	Tevatron Inclusive Jets . . . . .	16
4.3	Jet and Drell-Yan data . . . . .	18
<b>5</b>	<b>The <math>W</math> asymmetry at the LHC</b>	<b>20</b>
5.1	Inclusion of individual experiments . . . . .	20
5.2	Combination of ATLAS and CMS data . . . . .	24
<b>6</b>	<b>Global PDFs including LHC data</b>	<b>26</b>
6.1	Tevatron $W$ asymmetry data . . . . .	26
6.2	Combining LHC and Tevatron $W$ asymmetry data . . . . .	26
<b>7</b>	<b>Conclusions and outlook</b>	<b>32</b>

# 1 Introduction

In a series of previous papers [1–9], we constructed increasingly accurate sets of parton distributions (PDFs), using a Monte Carlo approach coupled to the use of neural networks as underlying interpolating functions. By definition, a PDF set provides a representation of a probability density in the space of parton distributions, i.e. a probability density in a space of functions [10–12]. We have performed various tests that confirm that NNPDF parton sets do indeed behave in a way which is consistent with the desired statistical properties of functional probability densities.

An advantage of providing a Monte Carlo representation of this PDF probability density is that new information (such as might be provided by new experimental data) can be included, using Bayes’ theorem, by reweighting an existing PDF set, without having to perform a new PDF fit [13, 14]: it is possible to determine a reweighting factor for each Monte Carlo replica in such a way that the information contained in the new data is included by simply computing weighted averages. This approach was first successfully developed and implemented in Ref. [14], where it was explicitly shown, in studies involving CDF and D0 inclusive jet data, that results obtained by reweighting are equivalent to those found by including the new data in the fit.

Reweighting takes a set of equally likely PDF replicas generated by importance sampling, and assigns to them weights reflecting their relative probabilities in the light of new data not included in the original fit. In this paper we develop a second technique, which we call ‘unweighting’, which takes the reweighted set and replaces it with a new set of replicas which are again all equally probable. This new set of replicas can then be used in precisely the same way as a fitted set. Even though no new information is gained by unweighting, presenting reweighted PDFs in the same form as a corresponding refitted set has various obvious practical advantages.

Furthermore, unweighting allows us to perform a highly nontrivial test of the reweighting procedure: namely, we take *two* new independent datasets, and use them to sequentially improve an existing set of replicas. This may then be done in either order, or indeed by treating them as one (combined) dataset. All three methods should yield equivalent results. Checking that this is the case provides a strong test of the method. However this can only be done if after each reweighting we unweight, because our simple closed-form expression for the weights can only be used for the reweighting of an equally probable (i.e. unweighted) set of PDFs.

We perform this check by first taking the NNPDF2.0 NLO DIS+DY fit [7], based on deep-inelastic and Drell-Yan data only, and taking as new datasets the CDF [15] and D0 [16] Run II inclusive jet data. This completes and refines the studies of Ref. [14], where it was verified that the inclusion of the combined CDF+D0 jet data by reweighting or refitting gives equivalent results. We then perform a second check using as the prior the NNPDF2.1 DIS fit [8], based on deep-inelastic data only, and taking as new datasets the E605 [17] Drell-Yan and Tevatron inclusive jet data. This provides a somewhat different test, because while the D0 and CDF data used in the previous test measure the same observable in the same kinematic region, the Drell-Yan and jet data affect different PDFs in different kinematic regions.

Besides its practical usefulness, the combined reweighting plus unweighting procedure is important because it allows one, at least in principle, to perform a global PDF fit by sequentially including new data by reweighting a generic prior distribution of PDFs [13]. If

the information contained in the new data is sufficiently precise, and the prior distribution sufficiently broad, the results will be largely independent of the prior one starts from: this would then give completely unbiased PDFs. In practice, this procedure is unlikely to be viable because, in order to get accurate results, the prior set of PDF replicas would have to be huge. However, the equivalence of PDFs obtained from reweighting with those determined using a fitting procedure (such as the NNPDF sets) confirms that the latter are also unbiased.

Following the success of these consistency tests, we use reweighting to evaluate the impact on the NNPDF2.1 NLO fit Ref. [8] of recent LHC data on the  $W$ -lepton asymmetry from the ATLAS and CMS collaborations. Using unweighting, we are able to produce a new PDF set, NNPDF2.2, which incorporates the effect of these data and the older  $W$ -lepton asymmetry from D0.

The outline of this paper is as follows. In Sec. 2 we revisit the derivation of the reweighting method, in particular the determination of the weights in terms of the  $\chi^2$  of the fit of the new data to each replica, and we discuss some subtle issues that were not tackled in Ref. [14], related to the definition of the measure in data space and to the inclusion by reweighting of multiple data sets. Then, in Sec. 3 we present our method of unweighting reweighted PDF sets, to give a set of replicas which are all equally probable, and show that indeed the unweighted set is equivalent to the original reweighted set. We follow this in Sec. 4 with a study of the consistency of the combined reweighting and unweighting procedure, when applied to more than one dataset in turn. After this theoretical study, we turn to phenomenology by using the method to investigate the impact of LHC measurement of the  $W$  lepton asymmetry on PDFs. First, we show in Sec. 5 how these data reduce the PDF uncertainties of light quarks in the medium and small- $x$  region, providing the first solid constraints on PDFs from LHC data, and then in Sect. 6 we construct a new set of NLO PDFs, NNPDF2.2, which includes, on top of all the data used to determine NNPDF2.1 PDFs, also the D0  $W$  asymmetry data already discussed in Ref. [14] and the LHC data discussed in Sect. 5.

## 2 Reweighting

In this section we revisit the derivation of the weight formula for reweighting ensembles of PDFs. In particular we discuss some of the more subtle issues in the formal proof presented in Ref. [14]. The derivation of the formula for the computation of the weights is nontrivial because we are dealing with probability densities in multidimensional spaces. In particular we need to avoid the ambiguities that can appear when dealing with conditional probabilities with respect to an event of probability zero, the so-called Borel-Kolmogorov paradox [18]. The conditional probabilities need to be defined carefully as integrations of conditional probability densities over finite volumes, in the limit when these volumes are taken to zero.

### 2.1 Integration over the data space

Bayes' theorem can be stated in terms of probability densities:

$$\mathcal{P}(f|y)\mathcal{D}f\mathcal{P}(y)d^n y = \mathcal{P}(y|f)d^n y\mathcal{P}(f)\mathcal{D}f, \quad (1)$$

where  $\mathcal{D}f$  is the integration measure in the space of PDFs, and  $d^n y$  is the integration measure in the space of data. The latter is an  $n$ -dimensional real space, where  $n$  is the number of data points used for reweighting.  $\mathcal{P}(f)$  is the prior density in the space of the PDFs: it is represented by the set  $\{f_k\}$  of PDF replicas. These are all equally probable, e.g., the expected PDF is simply determined as the average over the set  $\{f_k\}$ , and are determined by importance sampling by starting from experimental data [11].  $\mathcal{P}(f|y)$  is instead the new probability density, given the  $n$  data points  $y$ . Note that here, unlike in Ref. [14], we do not make explicit the dependence of conditional probabilities on generic prior information  $K$  (which includes the data used to determine the prior PDF, external parameters such as  $\alpha_s$ , and theoretical assumptions such as the use of perturbative QCD at a given order).  $\mathcal{P}(y)$  is the prior density in the space of data, and we do not need to specify its explicit form, since it can be fixed by requiring  $\mathcal{P}(f|y)$  to be correctly normalised. The only relevant property of  $\mathcal{P}(y)$  is that it does not depend on the PDFs  $f$ .

In order to *define* the probability density  $\mathcal{P}(f|y)$  at a given point  $y$ , we can integrate Eq. (1) in a small sphere  $S_\epsilon$  of radius  $\epsilon$  centered at  $y$ . Integrating the left-hand side of Eq. (1) over  $S_\epsilon$  we obtain

$$\int_{S_\epsilon} \mathcal{P}(f|y')\mathcal{D}f\mathcal{P}(y')d^n y' = [n^{-1}\epsilon^n\Omega_n\mathcal{P}(y)] \mathcal{P}(f|y)\mathcal{D}f, \quad (2)$$

where  $\Omega_n$  is the solid angle in  $n$  dimensions. Integrating the right-hand side similarly, we can cancel the volume factors on each side and thus take the limit  $\epsilon \rightarrow 0$ , to give

$$\mathcal{P}(f|y)\mathcal{D}f = \frac{\mathcal{P}(y|f)}{\mathcal{P}(y)}\mathcal{P}(f)\mathcal{D}f. \quad (3)$$

Now  $\mathcal{P}(y|f)$  is the likelihood density for the data  $y$ : assuming these data to be normally distributed about central values  $y[f]$  (which of course depend on the PDF  $f$ ),

$$\mathcal{P}(y|f) = (2\pi)^{-n/2}(\det\sigma)^{-1} \exp\left(-\frac{1}{2}(y-y[f])\sigma^{-1}(y-y[f])\right), \quad (4)$$

where  $\sigma$  is the experimental covariance matrix. The only dependence on  $f$  is through the value of

$$\chi^2(y, f) \equiv (y - y[f])\sigma^{-1}(y - y[f]). \quad (5)$$

It now follows from Eqs. (3-5) that

$$\mathcal{P}(f|y)\mathcal{D}f \propto \exp(-\frac{1}{2}\chi(y, f)^2) \mathcal{P}(f)\mathcal{D}f, \quad (6)$$

with a constant of proportionality that depends on  $y$ , but not on  $f$ , and can thus be fixed if necessary through the normalization condition  $\int \mathcal{P}(f|y)\mathcal{D}f = 1$ .

## 2.2 Weights for a given $\chi$

This is all fine so far as it goes, but is not sufficient to give us a reweighting of our ensemble of PDFs equivalent to a refitting. The reason for this is that when we fit PDFs, we do not demand that the predictions  $y[f]$  coincide with the data points  $y$ , but rather that the figure of merit  $\chi^2(y, f)$  is optimized. Thus rather than integrating both sides of Eq. (1) over the small spheres  $S_\epsilon$ , we should integrate over all  $y$  subject only to the single constraint that  $\chi^2(y, f) = \chi^2$ , for some fixed value  $\chi$ . It is convenient to choose as a parameter  $\chi$ , rather than  $\chi^2$ , because we can interpret  $\chi$  as the radial co-ordinate in a system of spherical polar co-ordinates in function space, centered at  $y' = y[f]$ .

The left-hand side of Eq. (1) thus becomes

$$\int \delta(\chi - \chi(y', f))\mathcal{P}(f|y')\mathcal{D}f \mathcal{P}(y')d^n y' \propto \mathcal{P}(f|\chi)\mathcal{D}f, \quad (7)$$

thus defining  $\mathcal{P}(f|\chi)$  up to an overall constant (independent of  $f$ ). We can evaluate it by performing the same integration over the right-hand side of Eq. (1), since the dependence on  $\mathcal{P}(f)$  factorises:

$$\int \delta(\chi - \chi(y', f))\mathcal{P}(y'|f)d^n y' \mathcal{P}(f) \mathcal{D}f = 2^{1-n/2}(\Gamma(n/2))^{-1}\Omega_n\chi^{n-1}e^{-\frac{1}{2}\chi^2} \mathcal{P}(f)\mathcal{D}f, \quad (8)$$

where we have used Eq. (4) for the likelihood, and performed the integral over  $y'$  in spherical co-ordinates. Comparing Eq. (7) and Eq. (8) we thus find

$$\mathcal{P}(f|\chi)\mathcal{D}f \propto \chi^{(n-1)}e^{-\frac{1}{2}\chi^2} \mathcal{P}(f)\mathcal{D}f. \quad (9)$$

In order to define the weight to be associated to each replica, we need to define the probability for each replica by integrating the probability density over a finite volume, and then send that volume to zero. For a given replica  $f_k$  we thus integrate  $\chi'$  over the region  $\chi_k < \chi' < \chi_k + \epsilon$ , where  $\chi_k = \chi(y, f_k)$ :

$$\int_{\chi_k}^{\chi_k + \epsilon} d\chi' \mathcal{P}(f_k|\chi') = \epsilon \mathcal{P}(f_k|\chi_k). \quad (10)$$

Note that this corresponds to integrating Eq. (7) over a spherical shell, centered on  $y[f_k]$ , of radius  $\chi_k$  and thickness  $\epsilon$ . The thickness of the shell is independent of the choice of replica: if it were not, we would bias the result.

It is easy to see using Eq. (9) that Eq. (10) gives the formula derived in Ref. [14] for the weights: since the replicas in the prior distribution all have equal probability,  $\mathcal{P}(f_k)$  is independent of the choice of replica  $f_k$ , and the weights are

$$w_k \propto \mathcal{P}(f_k|\chi_k) \propto \chi_k^{n-1} e^{-\frac{1}{2}\chi_k^2}. \quad (11)$$

The constant of proportionality may be fixed by normalizing the sum of the weights to the number of replicas.

The factor of  $\chi_k^{n-1}$  takes account of the fact that when there are many data points, larger values of  $\chi_k$  have a larger phase space available to them, while very small values are phase space suppressed: however good the model it is always very unlikely that the theoretical prediction will give exactly the right result for a large number of measurements. This is not a trivial result: it depends critically on choosing the correct volume upon which to integrate in the space of the new data  $y$ . Starting from the same probability density, but using a different integration volume would produce a different result. Hence we need to justify our particular choice of volume.

In this respect, we note that our choice includes all points in the space of  $y$  with a particular  $\chi^2$ , and that the thickness of the shell is independent of its radius  $\chi(y, f)$  or centre  $y[f]$ , in the same way that in Eq. (2) the radius of the little sphere was also independent of  $y[f]$ . The ultimate justification in both cases is that the probability measure  $d^n y$  on the space  $y$  is uniform, i.e. that equal volumes have equal probability: this assumption is of course implicit from the start, since without it the likelihood Eq. (4) would not be Gaussian.

Note that although the above argument is most naturally expressed using  $\chi$  as a coordinate in function space we would get the same weights  $w_k$  if we were to instead use  $\chi^2$ , or indeed a conditional dependence on any other monotonic function of  $\chi$ , so long as we use the same *volume* in the space of data to define the weights. To see this, note that for example

$$\mathcal{P}(f|\chi^2)\mathcal{D}f \propto \int \delta(\chi^2 - \chi^2(y', f))\mathcal{P}(f|y')\mathcal{D}f \mathcal{P}(y')d^n y', \quad (12)$$

so that, comparing with Eq. (7),

$$\mathcal{P}(f|\chi^2) = \mathcal{P}(f|\chi)/(2\chi). \quad (13)$$

As expected, we thus have  $\mathcal{P}(f|\chi)d\chi = \mathcal{P}(f|\chi^2)d\chi^2$ . If we work with  $\mathcal{P}(f|\chi^2)$ , in order to be sure to use the same volume in the space of data (i.e. a spherical shell of thickness  $\epsilon$ ) we must now integrate over the interval  $\chi_k^2 < (\chi')^2 < \chi_k^2 + 2\chi_k\epsilon$ :

$$w_k \propto \int_{\chi_k^2}^{\chi_k^2 + 2\chi_k\epsilon} d\chi'^2 \mathcal{P}(f_k|\chi'^2), \quad (14)$$

which then yields exactly the same weight Eq. (11) as obtained using Eq. (10).

### 2.3 Multiple experiments

Let us now discuss the implications of the above prescription for reweighting with more than one set of data. Suppose we are given a set of new data  $\{y\}$ , which is made of two *independent* subsets  $\{y_1\}$  and  $\{y_2\}$ , containing respectively  $n_1$  and  $n_2$  data points,

such as for example a dataset which includes results from two independent experimental measurements (of the same, or of different observables).

When the two sets of data are used for reweighting simultaneously, the only quantity that matters is the total  $\chi^2$  of the two experiments. Since we assumed the experiments to be independent,  $\chi^2 = \chi_1^2 + \chi_2^2$ , where  $\chi_i \equiv \chi(y_i, f)$ , and the probability density is therefore given by Eq. (9) above:

$$\mathcal{P}(f|\chi) \propto (\chi_1^2 + \chi_2^2)^{\frac{1}{2}(n_1+n_2-1)} e^{-\frac{1}{2}(\chi_1^2+\chi_2^2)}. \quad (15)$$

Clearly the individual values of  $\chi^2$  of the two sets need not each be fixed to  $\chi_1^2$  and  $\chi_2^2$ . Hence even though the likelihood factorizes,

$$\mathcal{P}(y_1 y_2 | f) = \mathcal{P}(y_2 | f) \mathcal{P}(y_1 | f), \quad (16)$$

the weights do not:

$$\mathcal{P}(f|\chi) \neq \mathcal{P}(f|\chi_2) \mathcal{P}(f|\chi_1). \quad (17)$$

Instead they are determined through the more complicated relation (see Eqs. (7) and (8))

$$\mathcal{P}(f|\chi) \propto \int \delta(\chi - (\chi_1^2 + \chi_2^2)^{1/2}) \mathcal{P}(y_2' | f) d^{n_2} y_2' \mathcal{P}(y_1' | f) d^{n_1} y_1'. \quad (18)$$

With Gaussian likelihoods Eq. (4), the integrals can be evaluated to give Eq. (15).

This means that if we wish to proceed sequentially, then after weighting with the first data set, with the usual weights  $\chi_1^{n_1-1} \exp(-\frac{1}{2}\chi_1^2)$ , the weights for the second data set are not given by

$$w_{2k} \propto \chi_{2k}^{n_2-1} \exp(-\frac{1}{2}\chi_{2k}^2), \quad (19)$$

but rather by

$$w_{2|1k} \propto (\chi_{1k}^2 + \chi_{2k}^2)^{(n_1+n_2-1)/2} \chi_{1k}^{-n_1+1} \exp(-\frac{1}{2}\chi_{2k}^2). \quad (20)$$

This perhaps appears odd at first sight, but is as it should be: the first dataset has altered the probability distribution of the PDFs, and thus the probabilities of the replicas before the second dataset can be considered must necessarily change. This is taken into account of by the dividing out the phase space factor of the first dataset, and multiplying by that of the combined dataset.

Nevertheless, it is possible to factorize the reweightings due to more than one dataset, if rather than attempting successive reweightings of the same set of replicas, one first turns the original weighted set into an unweighted set, and then computes the second set of weights using this set. This procedure will be discussed in detail in Sec. 4: however before we can do this we must first develop a procedure for unweighting.



### 3 Unweighting

In this section we present a method to unweight reweighted PDF sets so that they can be used without the need for including weights for individual replicas. The starting point is a set of  $N_{\text{rep}}$  reweighted replicas. Each replica, identified by the index  $k = 1, \dots, N_{\text{rep}}$ , carries a weight  $w_k$  defined in Eq. (11), determined by comparing each of the replicas of the original unweighted distribution to the new experimental information. Our goal is to unweight this PDF set in order to obtain a new set of  $N'_{\text{rep}}$  replicas with all weights equal to unity, but with the same probability distribution of the original weighted set, i.e. such that any moment of the probability distribution computed from the weighted and unweighted set would be the same in the limit in which  $N'_{\text{rep}} \rightarrow \infty$ .

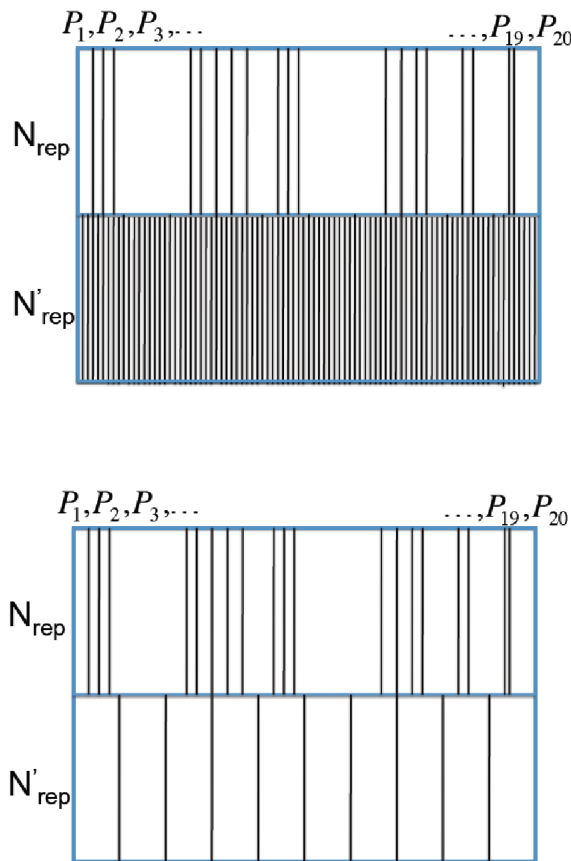


Figure 1: Graphical representation of the construction of a set of  $N'_{\text{rep}}$  unweighted replicas from a set of  $N_{\text{rep}} = 20$  weighted ones. Each segment is in one-to-one correspondence to a replica, and its length is proportional to the weight of the replica. The cases of  $N'_{\text{rep}} \gg N_{\text{rep}}$  (top) and  $N'_{\text{rep}} = 10$  (bottom) are shown.

### 3.1 The unweighting method

The basic idea for constructing the unweighted set consists of selecting replicas from the weighted set of  $N_{\text{rep}}$  replicas in such a way that replicas carrying a relatively high weight are chosen repeatedly, while those with vanishingly small weight disappear from the final unweighted set. The method is depicted graphically in Fig. 1. We start by subdividing a line of unit length into  $N_{\text{rep}}$  segments, in such a way that for each replica the length of the corresponding segment is proportional to the weight of the replica, and thus to its probability. The ordering of the segments is random. In order to extract a set of  $N'_{\text{rep}}$  replicas that faithfully represents this distribution, we draw another unit interval directly below the first, and subdivide it into  $N'_{\text{rep}}$  segments all of equal length  $1/N'_{\text{rep}}$ . We then select replicas from the original weighted set by taking a number of copies of each replica equal to the number of lower segments whose right edge is contained in the upper segment corresponding to that specific replica. A little thought shows that the (all equally probable)  $N'_{\text{rep}}$  replicas in the lower set are then chosen according to the probabilities of the  $N_{\text{rep}}$  replicas in the upper set.

To see this, note that, if the number of  $N'_{\text{rep}}$  replicas is large enough, (top plot in Fig. 1) then at least one lower segment (width  $1/N'_{\text{rep}}$ ) will be contained in each upper segment, and the original probability distribution is reproduced. This case is however unrealistic, as it would require  $N'_{\text{rep}}$  to be as large as the ratio between the highest and lowest weight, which can be very large indeed. It is also unnecessary, because the amount of information carried by the weighted set is measured by its Shannon entropy, which can be used to determine the effective number of unweighted replicas  $N_{\text{eff}}$  which carry the same information [14]. Hence, it is pointless to include a number of replicas  $N'_{\text{rep}}$  significantly larger than  $N_{\text{eff}}$ , as no information is then gained. Because by construction  $N_{\text{eff}} \leq N_{\text{rep}}$  the more realistic situation is depicted in the bottom plot of Fig. 1: for the larger weights several unweighted segments are contained in a weighted one, but for the smaller weights there are often none at all, since we only select a replica if the edge of a lower segment is contained in the upper segment corresponding to that replica. Which replica is chosen among many all with equally small weight is of course entirely random, since the ordering of the replicas is random.

We can now formulate the unweighting algorithm quantitatively. We start with a set of  $N_{\text{rep}}$  replicas, each carrying a weight  $w_k$  Eq. 11; as in Ref. [14], we normalize the weights according to

$$\sum_{k=1}^{N_{\text{rep}}} w_k = N_{\text{rep}}. \quad (21)$$

The probability of each replica is determined given its weight as

$$p_k = \frac{w_k}{N_{\text{rep}}}. \quad (22)$$

We then define probability cumulants

$$P_k \equiv P_{k-1} + p_k = \sum_{j=0}^k p_j, \quad (23)$$

where in the last step we take  $P_0 = 0$ . By construction,  $0 \leq P_k \leq 1$  and  $P_{k-1} \leq P_k$ . Indeed, the cumulants provide the co-ordinate of the edge of the  $k$ -th upper segment in the plot of Fig. 1, with origin at the left edge of the unit interval.

The unweighted set is then constructed as follows. We start with  $N_{\text{rep}}$  weights  $w_k$ , and we determine  $N'_{\text{rep}}$  new weights

$$w'_k = \sum_{j=1}^{N'_{\text{rep}}} \theta\left(\frac{j}{N'_{\text{rep}}} - P_{k-1}\right) \theta\left(P_k - \frac{j}{N'_{\text{rep}}}\right). \quad (24)$$

The weights  $w'_k$  are either zero or positive integers, and they satisfy the normalization condition

$$N'_{\text{rep}} \equiv \sum_{k=1}^{N_{\text{rep}}} w'_k : \quad (25)$$

in fact, they correspond to the graphical counting procedure described previously. The unweighted set is then simply constructed by taking  $w'_k$  copies of the  $k$ -th replica, for all  $k = 1, \dots, N_{\text{rep}}$ . The probability of replica  $k$  in the new unweighted set is then given by

$$p'_k = \frac{w'_k}{N'_{\text{rep}}}. \quad (26)$$

As a consequence we have

$$\lim_{N'_{\text{rep}} \rightarrow \infty} p'_k = p_k, \quad (27)$$

i.e. the unweighted set reproduces the probabilities of the weighted set in the limit of large sample size, as it ought to.

As already mentioned, even though exact identity of the reweighted and unweighted probability distribution holds in the limit Eq. (27), the amount of information contained in the weighted set corresponds to  $N_{\text{eff}} \leq N_{\text{rep}}$  unweighted replicas, with  $N_{\text{eff}}$  determined as in Eq. (10) of Ref. [14] from the Shannon entropy. Therefore for practical applications it is advisable to take  $N'_{\text{rep}} < N_{\text{eff}}$  — though there is nothing in principle wrong with taking  $N'_{\text{rep}} > N_{\text{eff}}$ , this would just lead to a highly redundant replica set. We will study the dependence of unweighted results on  $N'_{\text{rep}}$  in an explicit example below.

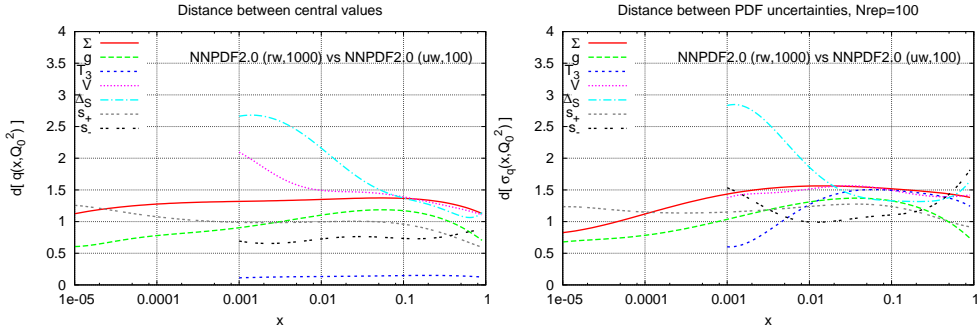


Figure 2: Distance between central values (left) and uncertainties (right) of the reweighted and unweighted PDFs determined from  $N_{\text{rep}} = 1000$  replicas of NNPDF2.0 DIS+DY reweighted with Tevatron jet data, as described in the text. The corresponding distances between refitted and reweighted PDFs were shown in Fig. 2 of Ref. [14].

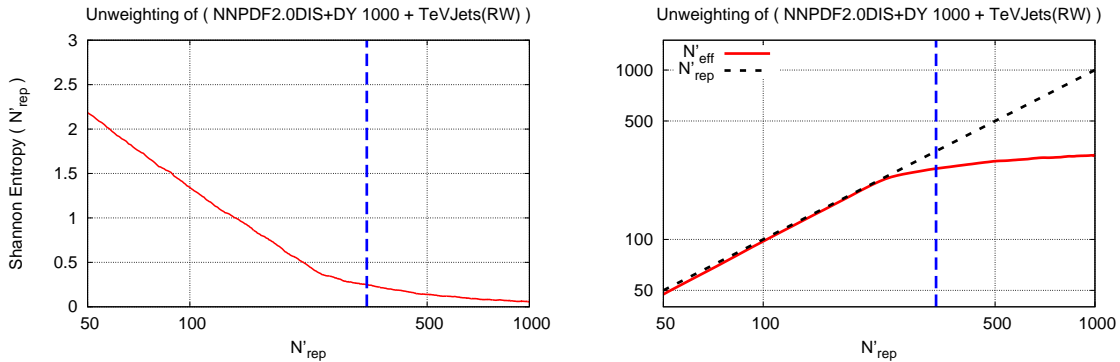


Figure 3: Left: the relative Shannon entropy  $H_R(N'_{\text{rep}})$  Eq. (28) as function of  $N'_{\text{rep}}$  for the reweighted and unweighted PDFs described in the caption of Fig. 2. Right: the effective number of replicas of the unweighted set  $N'_{\text{eff}}$  as function of  $N'_{\text{rep}}$ . The dashed vertical line denotes the value  $N'_{\text{rep}} = N_{\text{eff}}$ . In all plots a moving average of 25 replicas has been performed to smooth out random fluctuations.

### 3.2 Testing unweighting

As a proof of concept of the unweighting technique, we will apply it to the two cases discussed in Ref. [14]: the reweighting of NNPDF2.0 DIS+DY with Tevatron inclusive jet data and the reweighting of NNPDF2.0 with the D0 muon and inclusive electron  $W$  lepton asymmetry data.

First, we consider the reweighting of NNPDF2.0 DIS+DY [7] with the Tevatron inclusive jet data [15, 19]. As discussed in Ref. [14], starting with  $N_{\text{rep}} = 1000$  NNPDF2.0 DIS+DY replicas, after reweighting with jet data the effective number of replicas is  $N_{\text{eff}} = 334$ . A reasonable choice for the size of the unweighted set would be any number less than this: here we chose  $N'_{\text{rep}} = 100$ . We perform the unweighting following the procedure discussed above. The comparison between the reweighted PDFs and the unweighted set can be made quantitative by determining the distances between PDFs and uncertain-

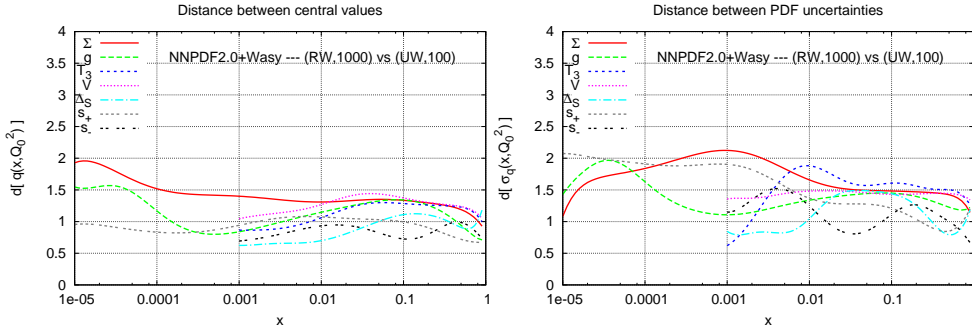


Figure 4: Distance between central values (left) and uncertainties (right) of the reweighted and unweighted PDFs determined from  $N_{\text{rep}} = 1000$  replicas of NNPDF2.0 DIS+DY reweighted with D0  $W$ -lepton asymmetry data, as described in the text.

ties. Distances were defined in Appendix A of Ref. [7], and in Ref. [14] in the weighted case; recall that distances  $d \sim 1$  correspond to statistically identical distributions, while (with  $N_{\text{rep}} = 100$  replicas)  $d \sim 7$  corresponds to distributions which are statistically inequivalent, but agree to one sigma. The distances between the reweighted PDF set and the same PDF set after unweighting are shown in Fig. 2. The corresponding distances between reweighted and refitted PDFs were shown in Fig. 2 of Ref. [14]. It is clear that the distances between reweighted and unweighted sets are generally smaller than those between the reweighted and the refitted sets, and they all fluctuate about  $d \sim 1$ , showing statistical equivalence (with the possible exception of the light sea asymmetry at small  $x$ , which is subject to very large uncertainties). We conclude that there is no significant loss of accuracy in the reweighting due to the unweighting.

We can now study the information contained in the unweighted set as the number of unweighted replicas  $N'_{\text{rep}}$  is varied. To this purpose, we compute the relative Shannon entropy between the unweighted set and the original weighted set, defined as

$$H_R(N'_{\text{rep}}) = \sum_{k=1}^{N_{\text{rep}}} p'_k \ln \frac{p'_k}{p_k}, \quad (28)$$

where  $p'_k$  are the probabilities Eq. (26), defined for each value of  $N'_{\text{rep}}$ . If the starting number of replicas  $N_{\text{rep}}$  is large enough that  $N'_{\text{rep}} \sim N_{\text{rep}}$  is already in the asymptotic region where Eq. (24) holds, then clearly for large  $N'_{\text{rep}} \sim N_{\text{rep}}$  the relative entropy  $H_R(N'_{\text{rep}})$  should fall to zero. For lower values of  $N'_{\text{rep}}$   $H_R(N'_{\text{rep}})$  measures the information loss between the original weighted set and the unweighted one.

In Fig. 3 we display  $H_R(N'_{\text{rep}})$ . It is clear that  $H_R(N'_{\text{rep}})$  falls linearly as a function of  $N'_{\text{rep}}$  up to  $N_{\text{eff}}$ , as more and more of the information in the weighted set is included. Around  $N'_{\text{rep}} \sim N_{\text{eff}}$  the slope of the fall changes abruptly, and  $H_R(N'_{\text{rep}})$  then falls slowly to zero as  $N'_{\text{rep}}$  increases, being already close to zero when  $N'_{\text{rep}} \sim N_{\text{eff}}$ . This can also be seen by computing directly the effective number of replicas  $N'_{\text{eff}}$  of the unweighted set as a function of  $N'_{\text{rep}}$ , which can be determined using Eq. (10) of Ref. [14], with the weights  $w'_k$  Eq. (24) and  $N = N_{\text{rep}}$ . Note that the result is nontrivial because some of the  $w'_k$  are zero, others are integers larger than one, and the dependence on  $N'_{\text{rep}}$  comes about only through the definition of the weights Eq. (24). The result is also shown in Fig. 3: at first

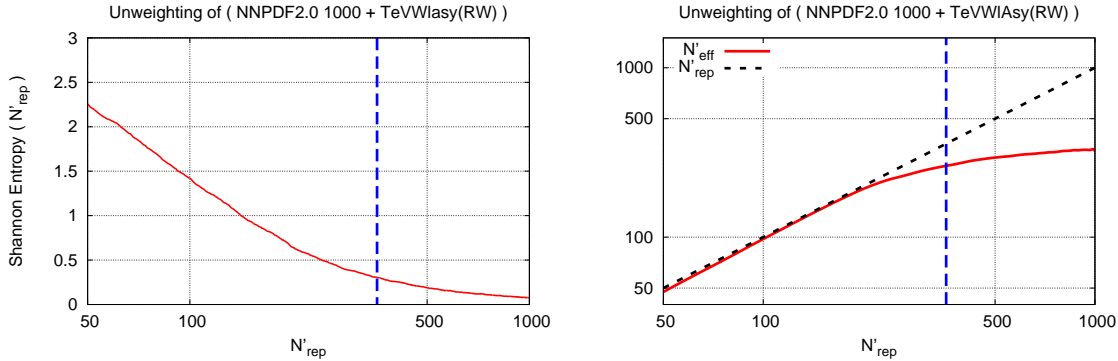


Figure 5: Same as Fig. 3, but for the pair of reweighted and unweighted PDFs described in the caption of Fig. 4.

$N'_{\text{eff}}$  grows linearly as a function of  $N'_{\text{rep}}$ , and is in fact very nearly equal to it. However when it reaches  $N'_{\text{rep}} \approx N_{\text{eff}}$ , the linear growth breaks off abruptly, and saturates at the value  $N'_{\text{eff}} = N_{\text{eff}}$ , which is reached asymptotically. Hence our expectation is borne out by these plots: the amount of information in the unweighted set increases with the number of unweighted replicas  $N'_{\text{rep}}$ , but only up to the point  $N'_{\text{rep}} \approx N_{\text{eff}}$ , after which nothing is gained by further increasing  $N'_{\text{rep}}$ .

We now repeat the same analysis for the unweighting of the NNPDF2.0 set, reweighted with the inclusive electron and muon D0 Run-II  $W$  lepton asymmetry data [20, 21]. The reweighting procedure for these data was presented in detail in Ref. [14]. The effective number of replicas, after reweighting a starting set of  $N_{\text{eff}} = 1000$  replicas, is in this case  $N_{\text{eff}} = 356$ . Again, we can choose the size of the unweighted set to be  $N'_{\text{rep}} = 100$ , as in the case above, and we perform the unweighting following the same procedure as before.

In Fig. 4 we show the distance between the reweighted and unweighted sets, and in Fig. 5 we plot the relative entropy between these two sets and the effective number of replicas in the unweighted set as a function of the number of unweighted replicas. The conclusions are the same as before: the unweighted set is indistinguishable from the reweighted one, provided that the number of unweighted replicas  $N'_{\text{rep}}$  is of the same order as the effective number of reweighted replicas  $N_{\text{eff}}$ . In the sequel we will thus feel free to use unweighted replica sets instead of their weighted counterparts, to which they are essentially equivalent.

## 4 Consistency

### 4.1 Multiple Reweighting

As we discussed in Sec. 2.3, when adding two new datasets to a set of prior PDFs, one way to proceed is to treat them as a single combined dataset, as in Eq. (15), i.e., with weights  $\chi^{(n-1)} \exp(-\chi^2/2)$  with  $\chi^2 = \chi_1^2 + \chi_2^2$  and  $n = n_1 + n_2$ . However, it should also be possible to treat them separately, weighting with first one dataset, then the other. If we do this using Eq. (20) then by construction we get the same answer that we would get by including the two sets at once, but this is trivial, because in the weights Eq. (20) the effect of the first weighting is divided out.

However, we can test non-trivially that two subsequent weightings by two independent datasets commute by incorporating the unweighting procedure. Formally we define the operation  $\hat{R}$  as reweighting with the weights given by Eq. (11), and an unweighting operation  $\hat{U}$ , as described in Sec. 3.1. Note that because the unweighting operator is a projection operator, it has no inverse. Weighting an existing PDF set by incorporating information from a new dataset then consists of the combined ‘weighting’ operation  $\hat{W} = \hat{U}\hat{R}$ . The weighting operation takes a set of replicas  $\{f_k\}$ , all equally probable, and replaces it with a subset which are again all equally probable, but the selection of which reflects information contained in the new dataset that was used in the reweighting  $\hat{R}$ . Clearly  $\hat{W}$  has no inverse, since it projects onto a lower dimensional space.

Now consider two datasets: the set of replicas produced by the action of weighting with the first dataset,  $\hat{W}_1$ , can be subject to a further weighting with the second dataset  $\hat{W}_2$ . Now of course the formula used to evaluate the weights used for the second reweighting must again be given by Eq. (11): the subset of replicas produced by  $\hat{W}_1$  are again all equally probable, so the second reweighting must work in precisely the same way as the first. The only difference is that  $\hat{W}_2$  acts only on those replicas produced by the action of  $\hat{W}_1$ .

Now for consistency it cannot matter in what order we perform these two weightings, and indeed their combined effect must be the same as for a single weighting  $\hat{W}_{12}$ , which treats the two datasets as a single dataset:  $\hat{W}_{12} = \hat{W}_2\hat{W}_1 = \hat{W}_1\hat{W}_2$ , or more explicitly

$$\hat{U}\hat{R}_{12} = \hat{U}\hat{R}_2\hat{U}\hat{R}_1 = \hat{U}\hat{R}_1\hat{U}\hat{R}_2. \quad (29)$$

So, for weighting to be consistent it must satisfy two nontrivial conditions: the combination property, and the commutation property. Clearly the first always implies the second (if  $\hat{W}_1\hat{W}_2 = \hat{W}_{12}$ , clearly  $\hat{W}_2\hat{W}_1 = \hat{W}_1\hat{W}_2$ , because  $\hat{R}_{12}$  is performed using weights determined through the total  $\chi^2 = \chi_1^2 + \chi_2^2$ ), but not the reverse (we might have  $\hat{W}_2\hat{W}_1 = \hat{W}_1\hat{W}_2 \neq \hat{W}_{12}$  if the formula Eq. (11) was incorrect).

In the remaining part of this Section we present two tests of the combination and commutation properties when two datasets are included. First, we consider sets of data for the same observable (the one-jet inclusive cross-section) in the same kinematic region by two different experiments. Then, we consider data for two different observables (a jet cross-section and a Drell-Yan cross section) which affect different PDFs in different kinematic regions.

	CDF	D0	CDF+D0
Data points	76	110	186
$N_{\text{eff}}$	290.8	565.8	334.5

Table 1: Datasets used in the Tevatron Run II inclusive jet reweighting exercise. For each set the number of data points and the effective number of replicas of the reweighted set of  $N_{\text{rep}} = 1000$  replicas are given.

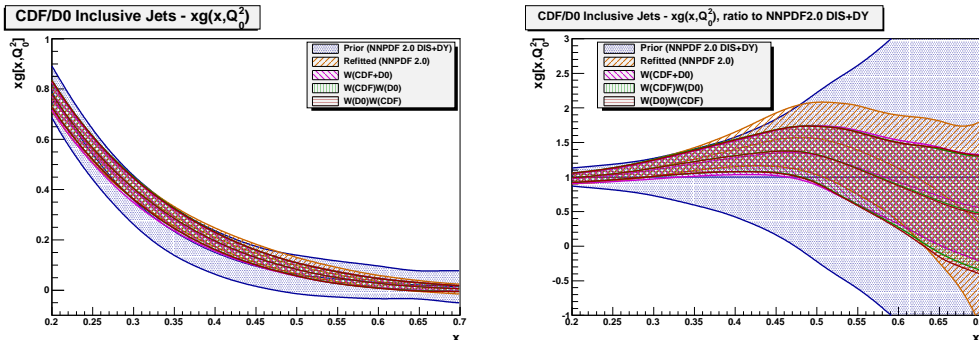


Figure 6: Comparison of the large- $x$  gluon PDF for prior set, reweighted sets with different successive reweighting orders and refitted set, when the jet data of Table 1 are included in the NNPDF2.0 NLO DIS+DY fit. Results are shown at  $Q^2 = 2 \text{ GeV}^2$ , both in absolute scale (left) and as a ratio to the prior (right).

## 4.2 Tevatron Inclusive Jets

The first exercise we present is an extension of the reweighting proof-of-concept in Section 4 of [14]. There, Run II Tevatron inclusive jet data production were included by reweighting a PDF set extracted from a NLO fit to DIS and Drell-Yan data (NNPDF2.0 DIS+DY) and the results compared to those obtained from a fit which included the same DIS, Drell-Yan and inclusive jet datasets all treated in the same way (NNPDF2.0).

In this Section we look again at the inclusion via reweighting of the same datasets, namely the CDF Run II- $k_t$  and D0 Run II-cone inclusive jet data in the NNPDF2.0 DIS+DY fit, but we now focus on comparing the results obtained in the following two cases:

- the two new datasets are included by reweighting the prior fit in a single step with both datasets;
- one of the datasets is included by reweighting, an unweighted set of PDFs is constructed using the procedure detailed in Section 3, and finally the latter set is reweighted again with the second dataset.

We will carry out the successive reweighting procedure (b) twice, exchanging the order in which the CDF and D0 datasets are included, in order to test the commutativity of the procedure. A final unweighting is performed for all the reweighted sets and the PDF comparisons and computations of distances are performed using these unweighted sets.

The number of data points and the effective number of replicas  $N_{\text{eff}}$  after reweighting with these data of a set of  $N_{\text{rep}} = 1000$  replicas are summarized in Table 1. In each



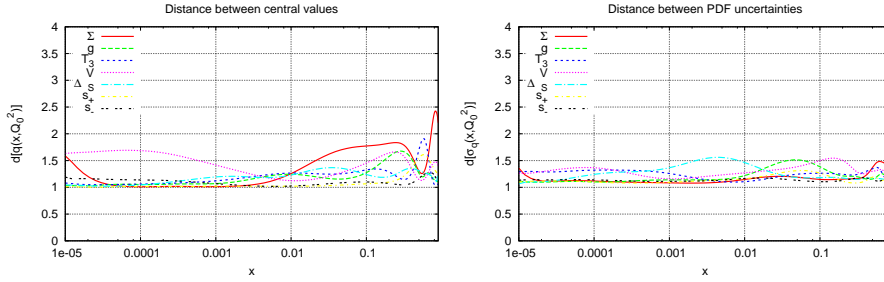


Figure 7: Distances between central values (left) and uncertainties (right) of PDFs from reweighting with the combined CDF+D0 dataset and PDFs from reweighting first with CDF data and then with D0 data.

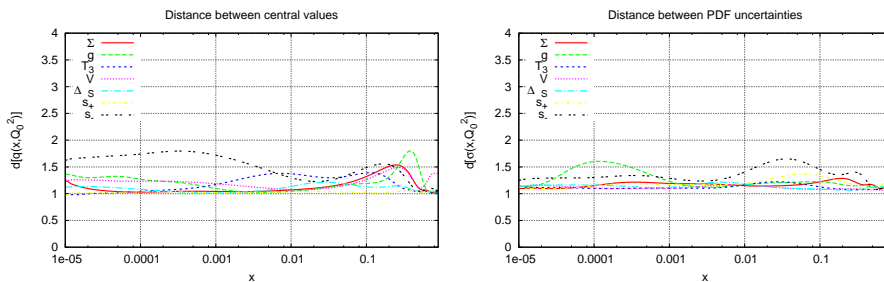


Figure 8: Distances between central values (left) and uncertainties (right) of PDFs obtained by reweighting with CDF and D0 jet data included in either order.

	(CDF+D0)	E605	(CDF+D0)+E605
Data points	186	119	305
$N_{\text{eff}}$	627.1	59.5	63.7

Table 2: As Tab. 1, but now for the E605 and inclusive jet reweighting exercise.

case, we construct a final set of  $N_{\text{rep}}^I = 100$  unweighted replicas. When the reweighting is performed in two steps, we first construct a (redundant) set of 1000 unweighted replicas, which is then reweighted and unweighted again to obtain the final set of 100 unweighted replicas.

As discussed in Refs. [7, 14], Tevatron jet data mostly affect the gluon at large  $x$ , leaving all other PDFs essentially unchanged. The impact of the inclusion of these data in the fit is shown in Fig. 6 where we compare the gluon for the prior set, the refitted one, and sets obtained reweighting the prior in the three different ways described above. As in the previous Section, a more quantitative assessment can be made by computing distances between various pairs of PDF sets. In Fig. 7 we show the distance between PDFs obtained by reweighting with the two sets at once and those found including CDF data first and D0 data next, while in Fig. 8 we show distances between sets obtained by including the CDF and D0 data in either order. It is clear that the three reweighting procedures lead to completely equivalent results.

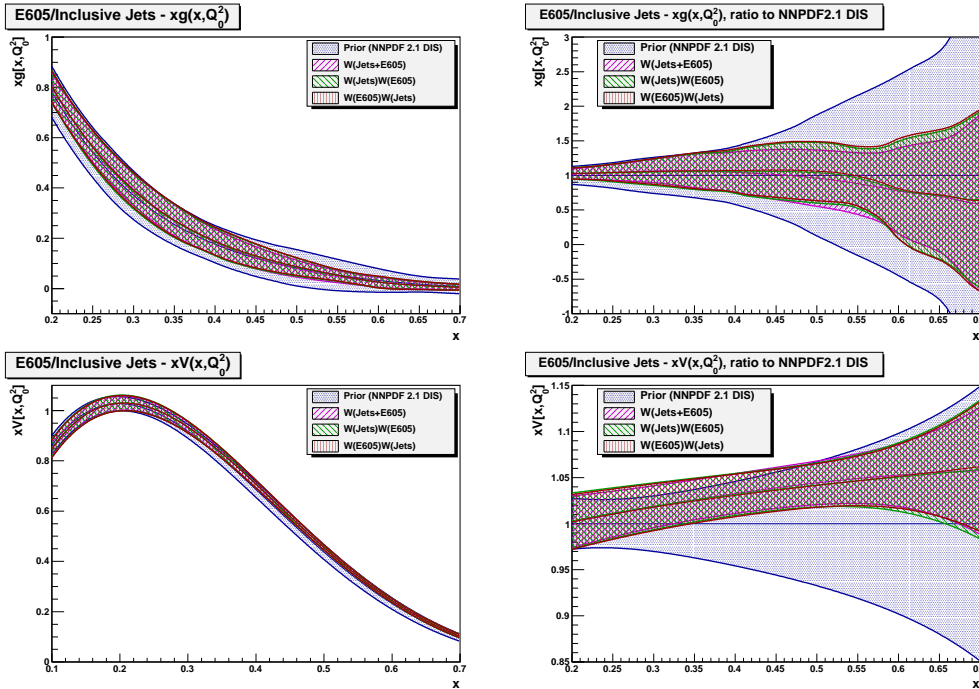


Figure 9: Comparison of the large- $x$  gluon and quark valence PDFs for prior set and reweighted sets with different successive reweighting orders, when the jet and Drell-Yan data of Table 2 are included in the NNPDF2.1 NLO DIS fit. Results are shown at  $Q^2 = 2 \text{ GeV}^2$ , both in absolute scale (left) and as a ratio to the prior (right).

### 4.3 Jet and Drell-Yan data

In this second exercise we start from a NLO fit to DIS data, NNPDF2.1 NLO DIS [8], and include the Tevatron inclusive jet data discussed in the previous section (D0 and CDF as a single dataset) and data from one of the Drell-Yan experiments which are included in the NNPDF2.1 global analysis (the E605 fixed target experiment [17]).

The number of data points and the effective number of replicas  $N_{\text{eff}}$  in this case are summarized in Table 2. Also in this case, we construct a set of  $N'_{\text{rep}} = 100$  unweighted replicas, with  $N'_{\text{rep}} = 1000$  unweighted replicas in the intermediate step if any. Note that this is a much less symmetric example than the previous one: the Drell-Yan data have a much greater impact than the jet data (in fact for the Drell-Yan data  $N'_{\text{rep}} > N_{\text{eff}}$ ).

As already mentioned, the jet data affect mostly the large  $x$  gluon, while the Drell-Yan data have mostly an impact on the quark flavour and antiflavour separation. The impact of these data on the gluon and the total quark valence distribution are shown in Fig. 9, where we show the results obtained by reweighting with the two sets included together, or one after another in either order. Note that in this case we do not have a refitted set. Distances between PDFs obtained by reweighting in the combined set, or first with jets then with Drell-Yan are shown in Fig. 10. Distances between PDFs obtained reweighting in either order are shown in Fig. 11. The test is clearly as successful here as it was in the previous case, despite being perhaps more challenging.

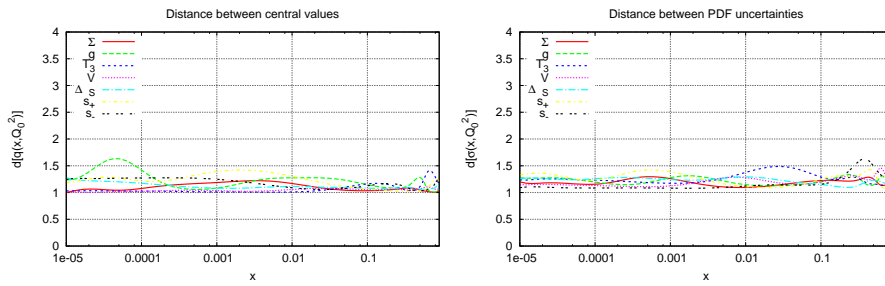


Figure 10: Distances between central values (left) and uncertainties (right) of PDFs from reweighting with the combined jet+Drell-Yan dataset and PDFs from reweighting first with jet data and then with Drell-Yan data.

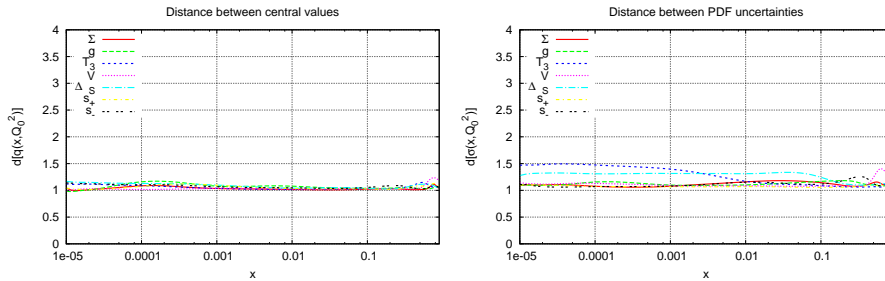


Figure 11: Distances between central values (left) and uncertainties (right) of PDFs obtained reweighting jet data and Drell-Yan data included in either order.

## 5 The $W$ asymmetry at the LHC

In this section we will use the reweighting technique presented here and in Ref. [14] to study the effect of including in the NNPDF2.1 NLO global fit the  $W$  lepton asymmetry measurements produced by the experimental collaborations at the LHC, and based on data collected in the 2010 run.

The  $W$  leptonic charge asymmetry is defined in terms of the  $W^\pm \rightarrow l^\pm \nu_l$  differential cross-sections  $d\sigma_{l^\pm}/d\eta$ , with  $\eta$  being the pseudorapidity of the lepton coming from the decay of the  $W$  boson, as

$$A_W^l = \frac{d\sigma_{l^+}/d\eta - d\sigma_{l^-}/d\eta}{d\sigma_{l^+}/d\eta + d\sigma_{l^-}/d\eta} \quad (30)$$

where the cross-sections are computed inside the acceptance cuts used to select the  $W \rightarrow l\nu_l$  events.

The ATLAS Collaboration published a first measurement of the muon charge asymmetry from  $W$  boson production in the pseudorapidity range  $|\eta| < 2.4$ , based on  $31\text{pb}^{-1}$  of accumulated luminosity [22], while CMS published a measurement of the muon and the electron charge asymmetries in the pseudorapidity range  $|\eta| < 2.2$ , based on  $36\text{pb}^{-1}$  of data [23]. The data provide a constraint for the above combination of PDFs in the region  $10^{-3} \lesssim x \lesssim 10^{-1}$ , where they are only partially constrained by the data already included in the NNPDF global analysis. In particular, while  $u$  is very well determined by fixed target DIS data,  $d$  and the light sea ( $\bar{d} - \bar{u}$ ) are currently much less constrained.

The LHCb collaboration presented preliminary results for a measurement of the muon charge asymmetry in the pseudorapidity range  $2 < |\eta| < 4.5$ , covered by the LHCb detector. This measurement probes PDFs in the small and large  $x$  regions, where data included so far in the global analyses provide much looser constraints. For this reason they might eventually have a substantially larger impact on global fits than the ATLAS or CMS data. However, at the time of writing these experimental results have only been presented in preliminary form [24], and are therefore not included in this study.

### 5.1 Inclusion of individual experiments

We begin by checking the compatibility of the individual ATLAS and CMS datasets for the charge lepton asymmetry with the data included in the NNPDF2.1 global fit, and by studying their impact when they are included separately in the fit using the reweighting technique presented in this paper.

The ATLAS muon charge asymmetry data [22] and CMS electron and muon data [23] are compared to the predictions obtained using three different NLO global fits, CT10 [25], MSTW2008 [26] and NNPDF2.1 in Fig. 5.1. The theoretical predictions including NLO QCD corrections are obtained using the fully differential Monte Carlo code DYNNLO [27] which allows for the implementation of arbitrary experimental cuts.

To give a more quantitative estimate of the level of agreement of the different predictions with the experimental data, in Table 3 we collect the  $\chi^2$  per number of data points for each individual dataset. Since no covariance matrix is provided by the LHC experiments at this point, we add statistical and systematic uncertainties in quadrature in the computation of the  $\chi^2$  values.

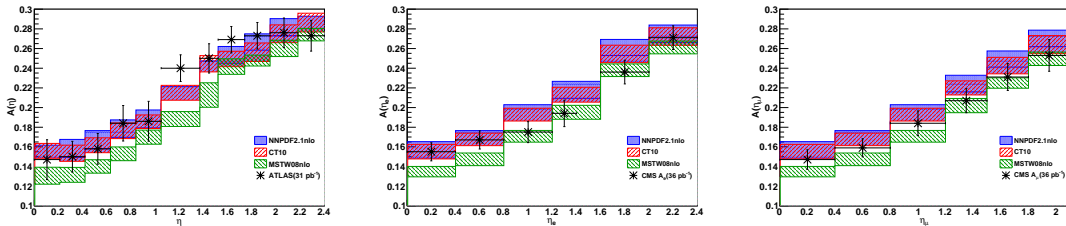


Figure 12: Predictions for the  $W$  lepton asymmetry at NLO, obtained with DYNNLO [27] using the CT10, MSTW08 and NNPDF2.1 parton sets, compared to measurements for the muon charge asymmetry from ATLAS [22] (left plot), and the electron (centre plot) and muon (right plot) charge asymmetries from CMS [23].

	$N_{\text{dat}}$	NNPDF2.1	CT10	MSTW08
ATLAS( $31\text{pb}^{-1}$ )	11	0.76	0.77	3.32
CMS( $36\text{pb}^{-1}$ ) electron $p_T > 25$ GeV	6	1.83	1.19	1.70
CMS( $36\text{pb}^{-1}$ ) muon $p_T > 25$ GeV	6	1.24	0.73	0.77

Table 3: Values of  $\chi^2/N_{\text{dat}}$  for the ATLAS and CMS lepton charge asymmetry data for different PDFs sets. Theory predictions are computed at NLO accuracy using the DYNNLO code. Note that in Ref. [22] a somewhat lower value is quoted for MSTW08, due to the use of the MC@NLO code.

The ATLAS muon charge asymmetry data are already very well described by the NNPDF2.1 prediction before being included in the analysis. This is shown by the excellent  $\chi^2/N_{\text{dat}} = 0.76$  reported in Table 3 and demonstrated by the distribution of  $\chi^2$  for the individual replicas before reweighting shown in the left plot of Fig. 13, which has a sharp peak around one. The compatibility of a new dataset with the data already included in a global analysis can be assessed by looking at the probability density for the parameter  $\alpha$ ,  $P(\alpha)$  defined in Eq. (12) of [14]. If this probability distribution peaks close to one, the new data are consistent with the ones already included in the global fit. For the ATLAS data, the  $P(\alpha)$  distribution, shown in the right plot of Fig. 13, is peaked slightly below one, thereby showing the good compatibility of these data with those included in the global analysis. Note that optimal values of  $\chi^2/N_{\text{dat}}$  are to be expected because statistical and systematic errors have been added in quadrature, thereby leading to an overestimation of uncertainties.

After reweighting NNPDF2.1 with the ATLAS data the quality of their description remains substantially unchanged, with the value  $\chi_{\text{rw}}^2/N_{\text{dat}} = 0.72$ . The number of effective replicas of the reweighted sets computed according to Eq. (42) in Appendix of [14] is  $N_{\text{eff}} = 928$ , out of the initial number of  $N_{\text{rep}} = 1000$  replicas in the prior. The distribution of the  $\chi^2/N_{\text{dat}}$  for the weighted replicas, shown in the center plot of Fig. 13, peaks just below one, again confirming the very good description of these data also after reweighting.

Given the outcome of the previous statistical analysis – a very good description of the data by the prior set to start with, resulting in a large number of surviving replicas ( $N_{\text{eff}} = 928$ ) – it is easy to predict that the ATLAS data alone will impose only mild

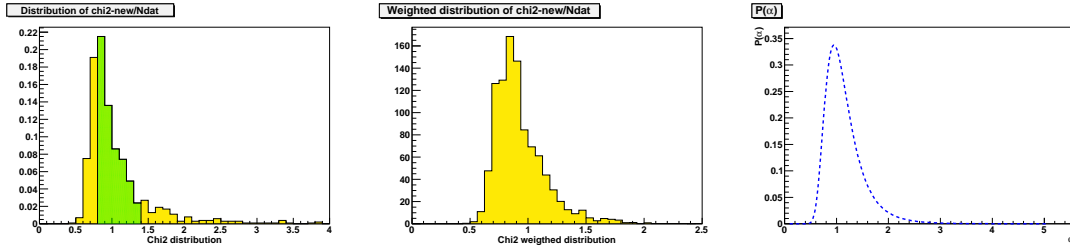


Figure 13: Distribution of  $\chi^2/N_{\text{dat}}$  for individual replicas prior (left) and after (middle) reweighting and  $\mathcal{P}(\alpha)$  distribution (right) for the ATLAS muon charge asymmetry data. In the left plot the shaded region corresponds to the central 68% of the distribution.

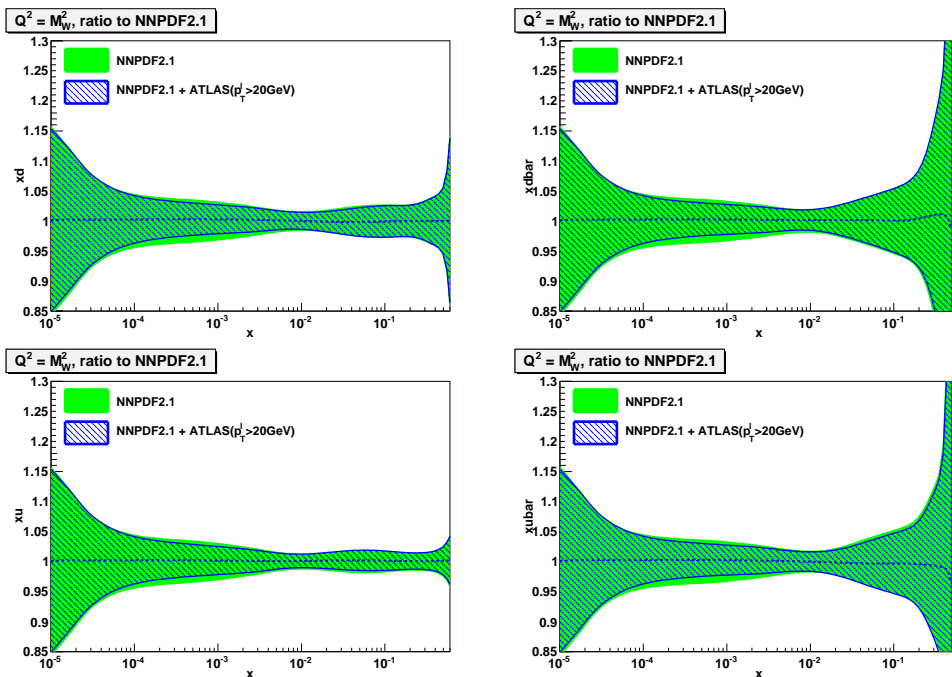


Figure 14: Comparison of light quark and antiquark distributions at the scale  $Q^2 = M_W^2$  from the global NNPDF2.1 NLO global fit and the same distributions obtained after adding ATLAS muon charge asymmetry data via reweighting. Parton densities are plotted normalized to the NNPDF2.1 central value.

constraints on the underlying PDFs. This is in fact what is seen in Fig. 14 where we compare the NNPDF2.1 light (anti)flavour densities at the scale  $Q^2 = M_W^2$  to the ones obtained after reweighting with the ATLAS data. The most noticeable effect is a reduction of the uncertainties on these PDFs in the medium-small  $x$  region, around  $x \sim 10^{-3}$ , by up to 20%.

We now turn to the CMS measurements described in [23]. CMS presented data for both the electron and muon charge asymmetries from  $W$  decays with two different cuts on the transverse momentum of the detected lepton:  $p_{\perp} > 25$  GeV and  $p_{\perp} > 30$  GeV. From the values for  $\chi^2/N_{\text{dat}}$  obtained using the NNPDF2.1 global set reported in Table 3, and the plots of the distribution of  $\chi^2/N_{\text{dat}}$  for individual replicas and of the  $\mathcal{P}(\alpha)$  distribution

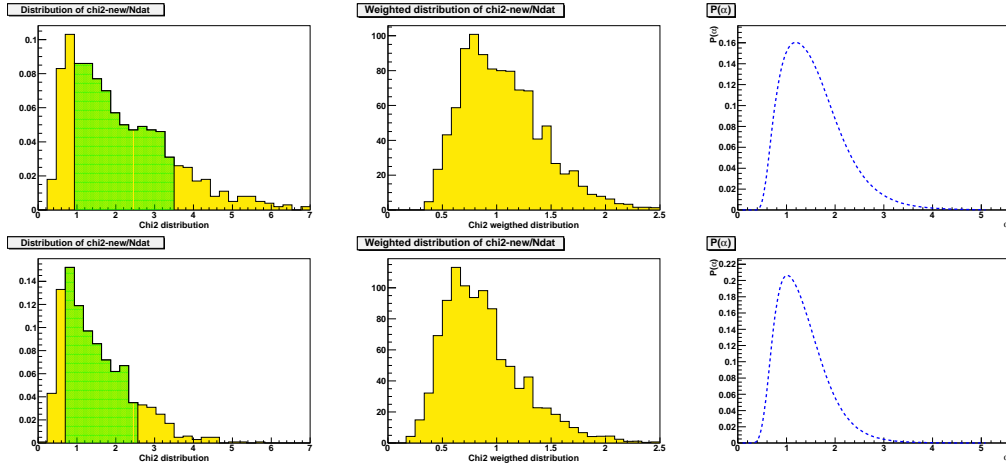


Figure 15: Same as Fig. 13 for the CMS( $p_T > 25$  GeV) (top) and CMS( $p_T > 30$  GeV) (bottom) lepton charge asymmetry data.

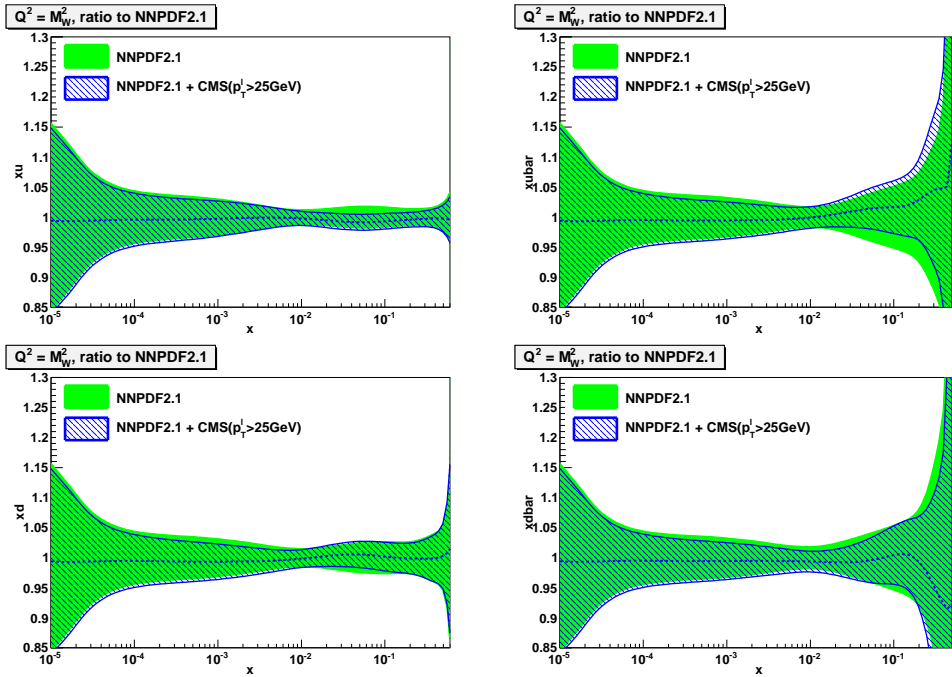


Figure 16: Same as Fig. 14 but after adding CMS lepton charge asymmetry data.

shown in Fig. 15, we see that both sets are equally well described by the NNPDF2.1 set and thus compatible with the data included in the global analysis. Since the two datasets are not independent we have to choose which one to use in our reweighting analysis and thus we only consider the dataset with the looser cut  $p_T > 25$  GeV, which proves to be more constraining of the PDFs. We perform our reweighting analysis including the muon and electron data as a single dataset.

The NNPDF2.1 prediction provides a good, though not optimal, description of the CMS data, as shown by the  $\chi^2/N_{\text{dat}} = 1.51$  obtained combining the values for the elec-

tron and muon data collected in Table 3. After reweighting, the description of these data improves significantly with  $\chi_{\text{rw}}^2/N_{\text{dat}} = 0.77$ . The number of effective replicas computed as above is roughly half the initial number of replicas,  $N_{\text{eff}} = 531$  out of  $N_{\text{rep}} = 1000$ , suggesting that these data will have a significant impact on the PDFs. The distribution of the  $\chi^2/N_{\text{dat}}$  of individual replicas after reweighting is centered around one, as shown in the middle-upper plot of Fig. 15.

The impact of the CMS data on light (anti)flavour PDFs, is shown in Fig. 16 where we observe a reduction of uncertainties in the medium  $x$  region smaller than that due to the ATLAS data, but also a change in the shape of the  $\bar{u}$  and  $\bar{d}$  distributions at relatively large  $x \sim 0.1$ , pushing up the central value a little and reducing the uncertainties by around 10% for the down distributions and as much as 25% for the up.

We conclude this Section by comparing the predictions for the charge asymmetry computed with NNPDF2.1 and NNPDF2.1 after reweighting with the ATLAS and CMS data respectively in Fig. 17. The effect on the prediction for the CMS data is more substantial, because the data undershoot the NNPDF2.1 NLO prediction in most of the higher rapidity bins.

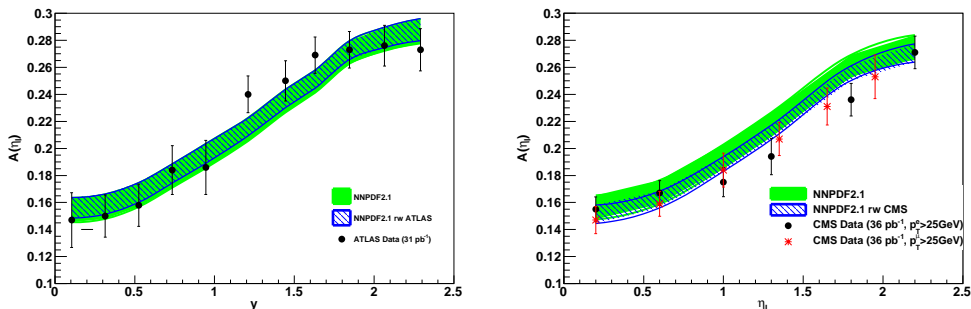


Figure 17: Comparison of the lepton charge asymmetry from  $W$  boson production computed with the NNPDF2.1 NLO PDF set and sets where ATLAS (left) and CMS (right) lepton charge asymmetry data have been included using reweighting.

## 5.2 Combination of ATLAS and CMS data

We now consider adding the ATLAS and CMS lepton charge asymmetry data as a single dataset to the NNPDF2.1 NLO global fit using reweighting.

The whole dataset is already well described by the NNPDF2.1 NLO dataset with  $\chi^2/N_{\text{dat}} = 1.17$  and the distributions of  $\chi^2/N_{\text{dat}}$  for individual replicas having a sharp peak around one, as shown by the left plot in Fig. 18. The compatibility of the ATLAS+CMS data with the data included in the global analysis and among the two experiments is also good, as can be deduced by looking at the  $\mathcal{P}(\alpha)$  distribution shown in the right plot in Fig. 18, which is nicely peaked around one.

After reweighting the description of the data improves, with  $\chi_{\text{rw}}^2/N_{\text{dat}} = 0.95$  with the distribution of  $\chi_{\text{rw}}^2/N_{\text{dat}}$  for individual replicas shown in the middle plot of Fig. 18 showing a sharp peak around one. These results, combined with the number of effective replicas surviving after reweighting, namely  $N_{\text{eff}} = 619$  out of the initial  $N_{\text{rep}} = 1000$ , show that the use of the ATLAS and CMS data together in the fit is not only possible but imposes



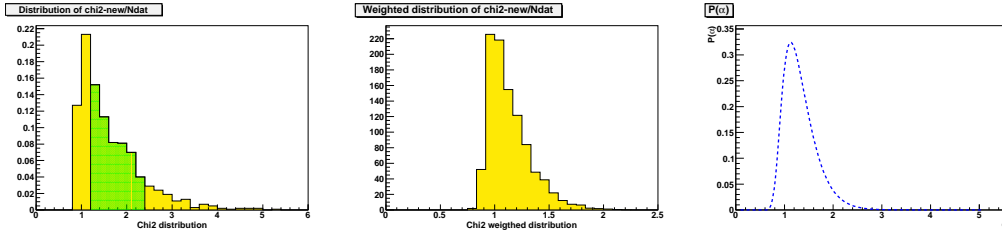


Figure 18: Same as Fig. 13 for the combined ATLAS+CMS ( $p_T > 25$  GeV) lepton charge asymmetry data.

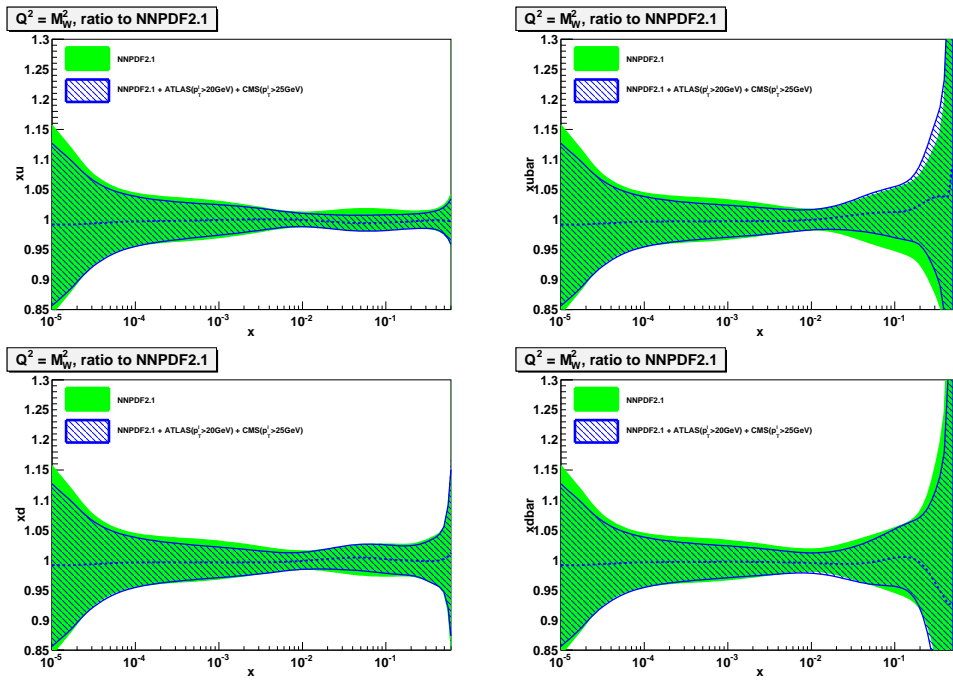


Figure 19: Same as Fig. 14 but after adding both the ATLAS and CMS lepton charge asymmetry data.

a moderate constraint on PDFs. However the constraint is not quite so great as with the CMS data alone, suggesting a mild incompatibility particularly in the high rapidity bins.

The impact of the data on the light flavour and anti-flavour distributions is shown in Fig. 19, where we compare the  $u$  and  $d$  quark and antiquark distributions at the scale  $Q^2 = M_W^2$  from the NNPDF2.1 global fit and the ones obtained after adding the ATLAS and CMS lepton charge asymmetry data using reweighting. There is around 20% reduction in uncertainties around  $x \sim 10^{-3}$ , mainly due to the ATLAS data, complemented by a reduction of between 10% and 25% at larger  $x$ , mainly due to the CMS data.

## 6 Global PDFs including LHC data

In this section we will check the consistency of the D0 and ATLAS+CMS datasets among themselves, and use both datasets to reweight the NNPDF2.1 NLO PDFs. The unweighting method presented in Sect. 3 is then used to produce a set of 100 unweighted replicas. The final product of this analysis is a new set of NNPDF parton distribution functions, NNPDF2.2 NLO, which includes, together with all the datasets already included in the NNPDF2.1 NLO global set, the D0, ATLAS and CMS lepton charge asymmetry data described above.

### 6.1 Tevatron $W$ asymmetry data

In Ref. [14] we used the reweighting technique to study the compatibility of the D0  $W$  lepton charge asymmetry data with the data included in the NNPDF2.0 NLO global fit and to assess their impact on the fitted parton densities. The conclusion of this study was that the data that are inclusive in the  $p_{\perp}$  of the identified lepton, namely the muon charge asymmetry data presented in [21] and electron charge asymmetry data with  $p_{\perp} > 25$  GeV released in [20], are consistent with each other and with all the other datasets included in NNPDF2.0, in particular with the CDF  $W$  asymmetry data [28] and the fixed-target DIS deuteron data. When included in the fit they have a moderate impact on PDFs, providing a reduction of the uncertainty of the valence quark distributions in the medium-high  $x$  region ( $x \sim 10^{-2}$ ).

Less inclusive electron charge asymmetry data were also presented in [20]. They are binned in  $p_{\perp}$ , divided into two sets with  $25\text{GeV} < p_{\perp} < 35\text{GeV}$  and  $p_{\perp} > 35\text{GeV}$  respectively. We observed [14] that these data, which could have potentially more impact on the PDFs, are inconsistent with some of the DIS data included in the global analysis and have problems of internal consistency. Similar conclusions have been reported by the MSTW [29] and CTEQ [25] collaborations, as they tried to include these datasets in the context of a PDF global analysis. We will thus not use these datasets here.

These results, though obtained using the NNPDF2.0 global fit, remain substantially unchanged if we use instead the NNPDF2.1 NLO global set as a prior fit to start the reweighting analysis. The muon charge asymmetry [21] and inclusive electron charge asymmetry data (with  $p_{\perp} > 25$  GeV) [20] can thus provide additional information to that from the ATLAS and CMS data considered in the previous section. We thus proceed directly to a combined fit of these data together with the LHC data.

### 6.2 Combining LHC and Tevatron $W$ asymmetry data

The description of the combined ATLAS, CMS and D0 charge asymmetry datasets obtained using the NNPDF2.1 NLO global fit, in which they were not included, is reasonably good but not optimal, with  $\chi^2/N_{\text{dat}} = 2.22$ : a detailed comparison is shown in Table 4. The distribution of the combined  $\chi^2/N_{\text{dat}}$  for individual replicas before and after reweighting, and the  $P(\alpha)$  distribution, shown in Fig. 20, indicate however that these data are reasonably compatible with the data already included in the NNPDF2.1 analysis and would provide a significant constraint on the PDFs.

These conclusions are indeed confirmed when the effect of the ATLAS, CMS and D0 data is included using the reweighting technique. After reweighting their overall description improves significantly, with a combined  $\chi_{\text{rw}}^2/N_{\text{dat}} = 0.81$ . This is due to a significant

Experiment	$N_{\text{dat}}$	NNPDF2.1	NNPDF2.1 LHC	NNPDF2.2
NMC-pd	132	0.97	0.95	0.97
NMC	221	1.73	1.72	1.72
SLAC	74	1.33	1.26	1.28
BCDMS	581	1.24	1.23	1.23
HERAI-AV	592	1.07	1.07	1.07
CHORUS	862	1.15	1.15	1.15
FLH108	8	1.37	1.37	1.37
NTVDMN	79	0.79	0.74	0.70
ZEUS-H2	127	1.29	1.28	1.28
ZEUSF2C	50	0.78	0.79	0.78
H1F2C	38	1.51	1.52	1.51
DYE605	119	0.84	0.84	0.86
DYE886	199	1.25	1.23	1.27
CDFWASY	13	1.85	1.81	1.81
CDFZRAP	29	1.66	1.61	1.70
D0ZRAP	28	0.60	0.60	0.58
CDFR2KT	76	0.98	0.98	0.96
D0R2CON	110	0.84	0.84	0.83
ATLASmuASY	11	[0.77]	0.97	1.07
CMSseASY	6	[1.83]	1.23	1.08
CMSmuASY	6	[1.24]	0.63	0.56
D0eASY	12	[4.39]	[3.46]	1.38
D0muASY	10	[1.48]	[1.17]	0.35
Total		1.165	1.158	1.157

Table 4: Table of  $\chi^2/N_{\text{dat}}$  values for the experiments included in the NNPDF2.1 NLO fit, the NNPDF2.1 LHC fit discussed in Section 5 and the NNPDF2.2 NLO fit. The numbers in square brackets correspond to the experiments which are not included in the fit. The three fits thus have respectively  $N_{\text{dat}} = 3338, 3361$  and  $3383$ .

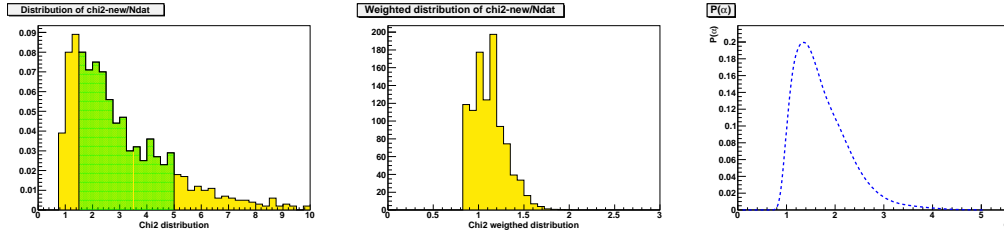


Figure 20: Same as Fig. 13 for the combined D0+ATLAS+CMS  $p_T > 25$  GeV dataset.

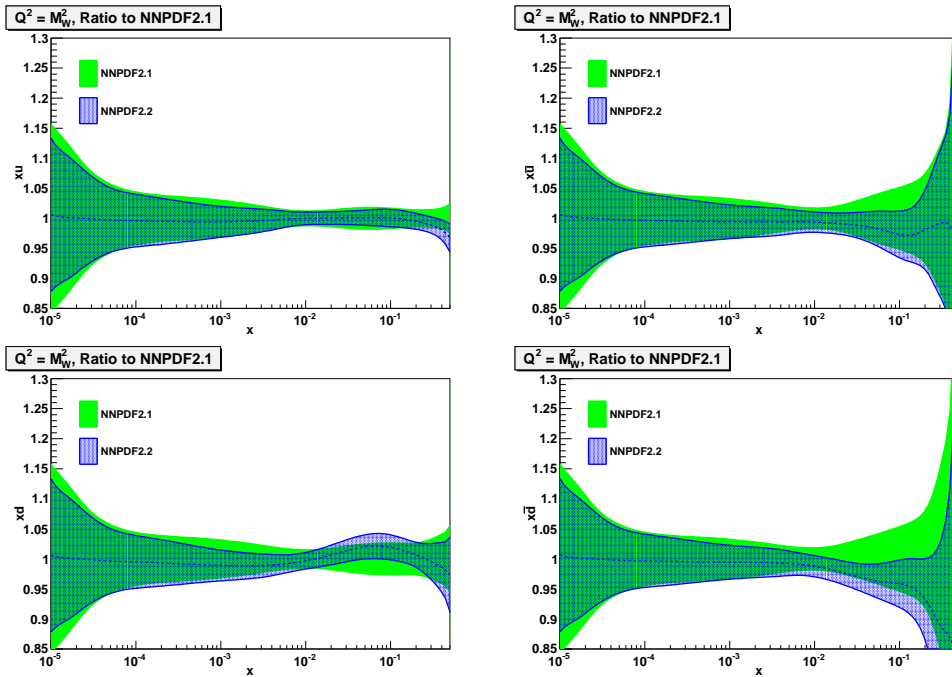


Figure 21: Comparison of light quark and antiquark distributions at the scale  $Q^2 = M_W^2$  from the global NNPDF2.1 and NNPDF2.2 global fits. Parton densities are plotted normalized to the NNPDF2.1 central value.

improvement in the fit to the CMS and the D0 data: the fit to the ATLAS data deteriorates a little, again showing that there is some tension. The number of effective replicas is now  $N_{\text{eff}} = 181$  out of the initial  $N_{\text{rep}} = 1000$ , showing that the  $W$  lepton asymmetry data indeed introduce very significant constraints on the PDFs. The distribution of the  $\chi^2/N_{\text{dat}}$  for the individual replicas after reweighting, shown in the middle plot of Fig. 20, is peaked around one, confirming the compatibility of these data with the other datasets included in the global analysis.

After reweighting, the unweighting procedure of Sec. 3 may be used to give a 100 replica set of PDFs equivalent to a global fit which includes all the data already included in NNPDF2.1, plus the ATLAS, CMS and D0  $W$  asymmetry data. We call this new NLO PDF set NNPDF2.2. The quality of the data to all the sets used in this new fit is shown in Tab. 4. There is no significant deterioration in the  $\chi^2$  in any of other datasets included in the global fit, and the fit to the NuTeV dimuon data improves significantly. The overall  $\chi^2_{\text{tot}}/N_{\text{dat}}$  thus also improves a little.

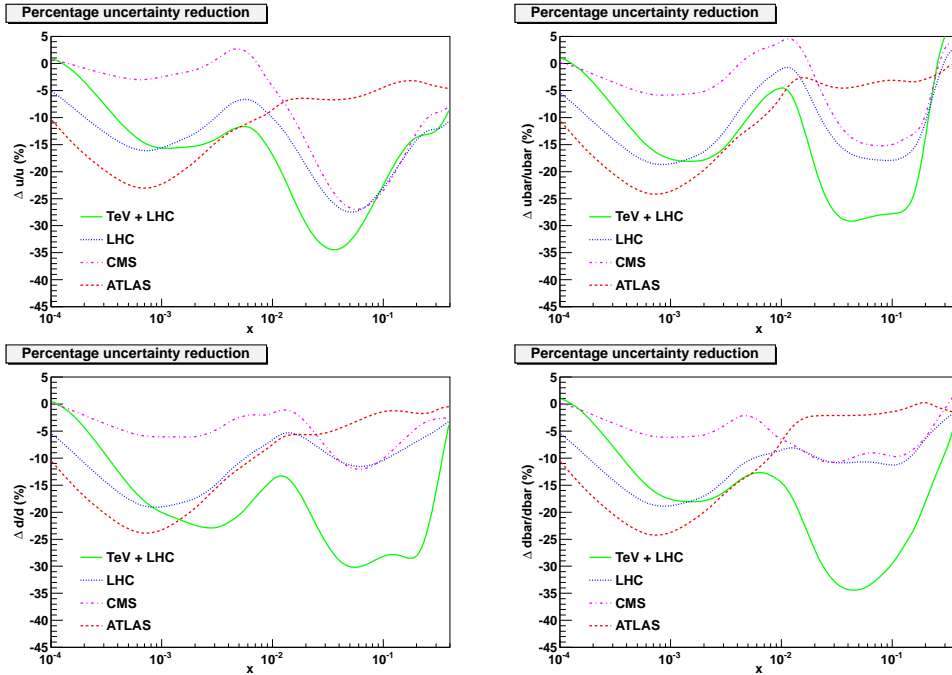


Figure 22: The percentage change in the uncertainty in the light quark and antiquark distributions at the scale  $Q^2 = M_W^2$  in the global NNPDF2.1 NLO global fit, after adding ATLAS, CMS and D0 lepton charge asymmetry data via reweighting. The four curves show in each case the effect of ATLAS (red) and CMS (pink) only, together (blue), and then together with the D0 data (green), i.e. NNPDF2.2.

The impact on light flavour and anti-flavour PDFs is shown in Fig. 21, where we compare the  $u$  and  $d$  quark and antiquark distributions at the scale  $Q^2 = M_W^2$ , from the NNPDF2.1 NLO set to the ones obtained for the NNPDF2.2 NLO set. The most noticeable effects of the inclusion of the new data are concentrated in two separate regions of  $x$ , namely, the  $x \sim 10^{-3}$  region, which is mostly affected by the ATLAS data, and the  $x \sim 10^{-2} - 10^{-1}$  region, which is mostly affected by the CMS and D0 data. In each of these regions, the  $W$  asymmetry data leads to a reduction of uncertainties on the light flavour and antiflavour distribution, or around 20% in the low  $x$  region, and up to 30% at higher  $x$  when CMS and D0 are combined (see Fig. 22). At higher  $x$  changes in the central values for these PDFs by up to one sigma are also observed: these are mainly due to the D0 data (compare Fig. 21 with Fig. 19).

As recently shown in the extensive studies carried out in the context of the PDF4LHC Working Group [30], there is rather good agreement among NLO parton distributions determined from the widest global datasets, specifically by the NNPDF, MSTW and CTEQ groups. However, there still are some significant differences, notably in the flavour separation at medium-large  $x$ . Since this is the region which is directly probed by the Tevatron and LHC lepton charge asymmetry data studied here, these data might help in resolving some of these outstanding incompatibilities.

To this end, in Figs. 23 and 24 we compare the  $d/u$  and  $(\bar{d} - \bar{u})$  combinations at the scale  $Q^2 = M_W^2$  obtained in the NNPDF2.1 and MSTW08 NLO global analyses, which do not include any of the  $W$  asymmetry data, the CT10 analysis, which includes only

the D0 data, and the new NNPDF2.2 fit, which also includes the ATLAS and CMS data. The new data lie in a region of  $x$  where the compatibility between the results obtained by different collaborations is at best marginal: in particular the  $d/u$  ratio given by MSTW08 is too low at large  $x$  and too high at medium  $x$ . The reduction of uncertainty when going from NNPDF2.1 to NNPDF2.2 is quite visible: the NNPDF2.2 prediction should thus be taken as the most reliable at present. Future LHC data will constrain the light quark PDFs in this region even more.

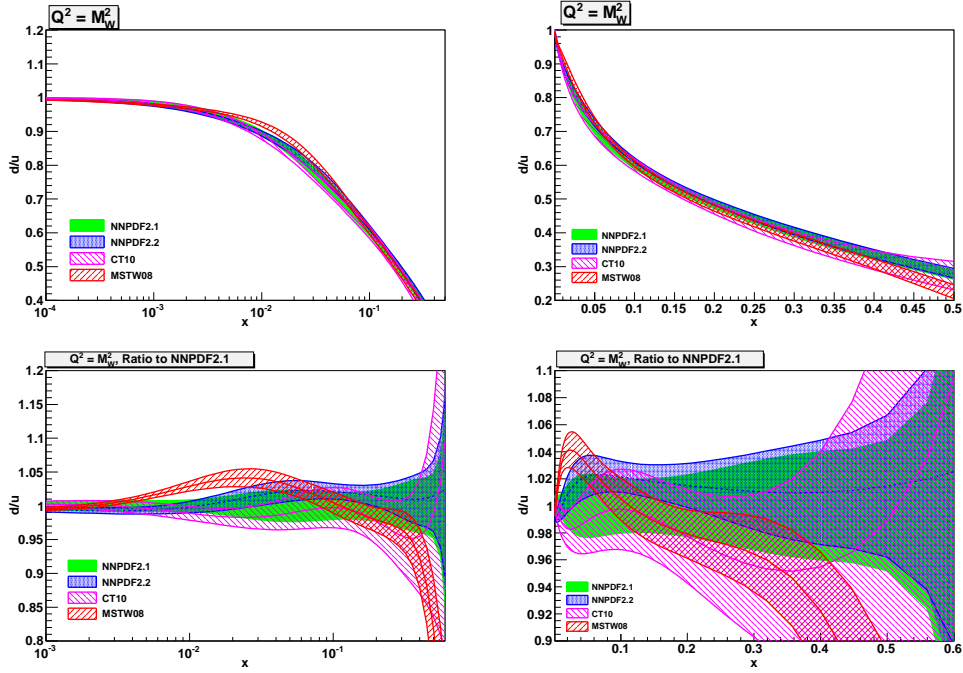


Figure 23: Comparison of the  $d/u$  ratio at  $Q^2 = M_W^2$  in NNPDF2.1, CT10, MSTW08 and NNPDF2.2. Upper plots show absolute values, while the lower plots show the ratio to NNPDF2.1

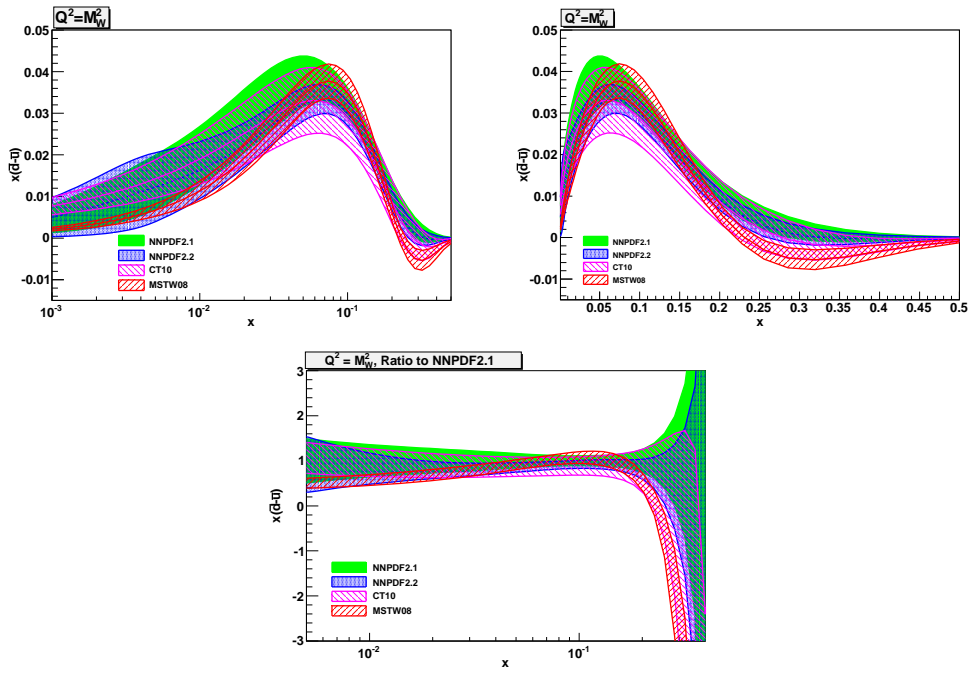


Figure 24: As Fig. 23, but showing  $(\bar{d} - \bar{u})$  at  $Q^2 = M_W^2$ .

## 7 Conclusions and outlook

The reweighting method which we have reviewed, re-derived and refined in this paper is a powerful technique which enables one both to perform interesting studies of the statistical properties of parton distributions viewed as probability distributions in a space of functions, and to rapidly and effectively include new experimental information in parton sets. Coupled to the unweighting method that we have presented and tested here it allows one to quickly upgrade existing Monte Carlo replica PDF sets to new sets which, while retaining the same format, include new experimental information.

The method has been used here to construct the NNPDF2.2 NLO PDF set — the first PDF set to include LHC data. This will doubtless be the first of many such sets: the quantity, quality and diversity of LHC measurements potentially relevant for PDF determination is now growing at an impressive rate.

---

The NNPDF2.2 NLO LO PDF set that has been presented in Section 6 is available from the NNPDF web site,

<http://sophia.ecm.ub.es/nnpdf>

and will be also available through the LHAPDF interface [31]:

- NNPDF2.2 NLO, set of  $N_{\text{rep}} = 100$  replicas:  
`NNPDF22_nlo_100.LHgrid`

---

## Acknowledgments

We are especially grateful to John Collins and Jon Pumplin for detailed questions and a critique of the reweighting method which largely stimulated this investigation. We thank Georgios Daskalakis, Gautier Hamel de Monchenault, Michele Pioppi, Michael Schmitt and Ping Tan for help with the LHC  $W$  asymmetry data, and Giancarlo Ferrera for help with the DYNLO code. LDD acknowledges the warm hospitality of the theory group at KMI, Nagoya, during the final stages of this work. RDB would likewise like to thank the Discovery Center at the NBI, Copenhagen. MU is supported by the Bundesministerium für Bildung und Forschung (BmBF) of the Federal Republic of Germany (project code 05H09PAE). We would like to acknowledge the use of the computing resources provided by the Black Forest Grid Initiative in Freiburg and by the Edinburgh Compute and Data Facility (ECDF) (<http://www.ecdf.ed.ac.uk/>). The ECDF is partially supported by the eDIKT initiative (<http://www.edikt.org.uk>).



## References

- [1] S. Forte et al., JHEP 05 (2002) 062, hep-ph/0204232.
- [2] The NNPDF Collaboration, L. Del Debbio et al., JHEP 03 (2005) 080, hep-ph/0501067.
- [3] The NNPDF Collaboration, L. Del Debbio et al., JHEP 03 (2007) 039, hep-ph/0701127.
- [4] The NNPDF Collaboration, R.D. Ball et al., Nucl. Phys. B809 (2009) 1, arXiv:0808.1231.
- [5] The NNPDF Collaboration, J. Rojo et al., (2008), arXiv:0811.2288.
- [6] The NNPDF Collaboration, R.D. Ball et al., Nucl. Phys. B823 (2009) 195, arXiv:0906.1958.
- [7] The NNPDF Collaboration, R.D. Ball et al., Nucl. Phys. B838 (2010) 136, arXiv:1002.4407.
- [8] The NNPDF Collaboration, R.D. Ball et al., Nucl. Phys. B849 (2011) 296, arXiv:1101.1300.
- [9] The NNPDF Collaboration, R.D. Ball et al., (2011), arXiv:1107.2652.
- [10] W.T. Giele, S.A. Keller and D.A. Kosower, (2001), hep-ph/0104052.
- [11] The NNPDF Collaboration, R.D. Ball et al., “Parton distributions: determining probabilities in a space of functions”, to be published in the proceedings of PHYSTAT 2011; CERN Yellow Report, 2011, arXiv:1110.1863.
- [12] S. Forte, Acta Phys. Polon. B41 (2010) 2859, arXiv:1011.5247.
- [13] W.T. Giele and S. Keller, Phys. Rev. D58 (1998) 094023, hep-ph/9803393.
- [14] The NNPDF Collaboration, R.D. Ball et al., Nucl.Phys. B849 (2011) 112, arXiv:1012.0836.
- [15] CDF - Run II, A. Abulencia et al., Phys. Rev. D75 (2007) 092006, hep-ex/0701051.
- [16] D0, V.M. Abazov et al., Phys. Rev. Lett. 101 (2008) 062001, arXiv:0802.2400.
- [17] G. Moreno et al., Phys. Rev. D43 (1991) 2815.
- [18] E. Jaynes, Probability Theory: The Logic of Science (Cambridge University Press, 2003).
- [19] CDF, T. Aaltonen et al., Phys. Rev. D78 (2008) 052006, arXiv:0807.2204.
- [20] D0, V.M. Abazov et al., Phys. Rev. Lett. 101 (2008) 211801, arXiv:0807.3367.
- [21] D0, V.M. Abazov et al., Phys. Rev. D77 (2008) 011106, arXiv:0709.4254.
- [22] ATLAS, G. Aad et al., (2011), arXiv:1103.2929.

- [23] CMS, S. Chatrchyan et al., JHEP 04 (2011) 050, arXiv:1103.3470.
- [24] LHCb, T. Shears, PoS EPS-HEP2009 (2009) 306.
- [25] H.L. Lai et al., Phys. Rev. D82 (2010) 074024, arXiv:1007.2241.
- [26] A.D. Martin et al., Eur. Phys. J. C63 (2009) 189, arXiv:0901.0002.
- [27] S. Catani et al., Phys. Rev. Lett. 103 (2009) 082001, arXiv:0903.2120.
- [28] CDF, T. Aaltonen et al., Phys. Rev. Lett. 102 (2009) 181801, arXiv:0901.2169.
- [29] R.S. Thorne et al., PoS DIS2010 (2010) 052, arXiv:1006.2753.
- [30] S. Alekhin et al., (2011), arXiv:1101.0536.
- [31] D. Bourilkov, R.C. Group and M.R. Whalley, (2006), hep-ph/0605240.